Volume 1 | Number 1 | Jan 2013 | Pages 1–100

PCCP

Physical Chemistry Chemical Physics
www.rsc.org/pccp

ROYAL SOCIETY OF CHEMISTRY

Journal Name

ARTICLE

Formation Mechanism of Ultra Porous Framework Materials

Pierre Fayon and Abbie Trewin[*]

Understanding the formation mechanism of ultra porous framework materials may lead to insights into strategies for the design and synthesis of novel ultra porous materials or for the increased surface area of known materials. Several potential formation mechanism have been proposed based on experimental evidence. Here, we assess, via simulation of the network generation process, these mechanisms and have identified key processes by which network interpenetration is minimised and hence surface area is maximised.

Introduction

Microporous materials, including metal-organic frameworks (MOFs)[1-3], covalent organic frameworks (COFs)[4-8], and microporous organic polymers (MOPs) have applications for gas adsorption, heterogeneous catalysis, and chemical separations.[9-13] COFs and MOFs are crystalline and can exhibit ultra high surface areas (Brunauer Emmett Teller (BET) surface areas over 6000 m^2 g^{-1})[14] with good thermal stabilities reported, although some studies suggest chemical decomposition, for example, of COF-1 in air. In contrast, MOPs, have been shown to be very robust with good physicochemical stabilities, for example towards water. MOPs have wide synthetic diversity available including hyper-crosslinked polymers (HCPs)[15], porous aromatic frameworks (PAFs)[16, 17], conjugated microporous polymers (CMPs)[18, 19] and polymers of intrinsic microporosity (PIMs).[20]

PAF-1 has a surface area of 5600 m^2 g^{-1} as obtained by analysis of the N$_2$ uptake isotherm using the BET equation. An open framework diamondoid topology was initially suggested. However, no evidence of structural order was observed and so alternative structure based upon amorphous silica was suggested.[21] This structure has an open framework and was able to rationalise the exceptionally high surface area and the structural characterisation data.

The mechanism by which PAF-1 is able to form an open framework structure is not known. Other MOP materials, including CMPs and HCPs, form denser interpenetrated network structures whereby the pore void space is formed through inefficient packing of the polymer net.[18, 22, 23] Several

^{a}· *Address here. Dept of Chemistry, Lancaster University, Lancaster, UK, LA1 4YB.*
† Footnotes relating to the title and/or authors should appear here.
Electronic Supplementary Information (ESI) available: [details of any supplementary information available should be included here]. See DOI: 10.1039/x0xx00000x

mechanisms of polymer network formation have been suggested, these include: (1) Instantaneous network formation: The monomer precursors form a gel-like state followed by an instantaneous reaction to form the polymer network;[24, 25] (2) Condensed step-by-step: The monomer precursors react to form oligomers which then form a gel-like state which then further react to form clusters of varying sizes. Phase separation of dense clusters leads to precipitation of spherical particles. Further inter-particulate cross-linking reactions form the polymer network;[26, 27] (3) Cluster step-by-step: A seed fragment of the network forms followed by step-by-step growth of the fragment to form a large cluster. The clusters conglomerate followed by precipitation and further cross-linking reaction to form the network;[28, 29] (4) Templating: A templating agent directs the formation of an open framework blocking the large pore voids from network interpenetration.[30]

Mechanistic studies of CMP materials have shown that these undergo network formation of type (2): Condensed step-by-step.[30] Network interpenetration occurs during the formation of the oligomers, at which point in the reaction a dense non-porous precipitate was found. At later stages of the reaction process, the clusters precipitate out of solution but continue to react to form a microporous powder. In contrast, PAF-1 is an open framework material and hence does not exhibit any network interpenetration and so the microporosity must arise during the early stages of the framework formation.

PAF-1 is formed via a Yamamoto[31] type Ullman cross-coupling reaction using a Ni(0) catalyst. The bis(1,5-cyclooctadiene)nickel(0) (Ni(COD)$_2$ or Ni(0)Lm) catalyst undergoes oxidative addition to a halogen functionalised monomer, **2**. Two of these **2** complexes undergo disproportionation to form **3**, followed by reductive elimination resulting in the addition products.[32] Figure 1 shows the overall catalytic reaction mechanism. The step that plays an important role in the structural topology of the polymer is

the disproportionation mechanism by which two of **2** disproportionate to give Ni(COD)$_2$Br$_2$ and **3**. The exact structural mechanism of the disproportionation reaction has not been characterised due to it being an extremely fast reaction. For similar reactions involving NiBPY complexes, a dimer is formed where either bridging phenyl or bridging halide group is present.[33] The mechanism proceeds by exchange of the Br and organic ligands to give **3** and Ni(COD)$_2$Br$_2$, outlined in Figure 2. The disproportionation mechanism is thought to occur via a parallel concerted exchange of ligands. During the first stages of the framework formation, the orientation of the PAF build units relative to each other will not be important, as they can easily re-orientate in solution to the preferable orientation. Whereas once the framework has formed and the PAF build units are fixed in position relative to the catalyst, then the relative orientation of the two PAF build units with respect to each other becomes more influential. At this stage of the framework formation there are two potential mechanisms possible; mechanism A, whereby a unit of **2** in solution is able to orientate itself relative to a unit of **2** that is bound to the framework in such a way that disproportionation between the two units of **2** is able to occur; and mechanism B, whereby two units of **2** that are bound to the framework are located and orientated in such a way that disproportionation between the two units of **2** is able to occur. Mechanism B can only occur when a framework cluster has formed at which point both Mechanism A and B can occur. Mechanism A results in framework growth whereas Mechanism B results in addition reaction within the existing framework. In both Mechanism A and Mechanism B the optimal orientation is when both Ni complexes are parallel and facing in the same direction. This is in direct contradiction to the expected end-to-end mechanism often envisaged when constructing computational models of amorphous polymer networks and framework systems.

Here, we attempt to identify the mechanism by which the open framework structure of PAF-1 is formed and thus suggest strategies towards the synthesis of new ultra high surface area polymer framework materials.

Computational Methodology

The key step in the Yamomoto cross-coupling is the disproportionation of two of the Ni(COD)$_2$BrR to result in Ni(COD)$_2$R$_2$. A model of the **2** intermediate was generated using the *Material Studio Modelling 5.0* package (Accelrys Inc. San Diego, CA, 2009). The geometry was optimised using NWChem 6.1 with the 6-311G basis set and B3LYP functional and incorporating the Grimme dispersion correction.[34, 35] The resulting structure informs the structural parameters used in the following structure generation strategies.

In previous studies, we described an automated computational code, called AMBUILD and written in Python, that was used to generate a PAF-1 framework model.[21] A PAF building block was generated based on the tetrakis (4-bromophenyl) methane. An end group is assigned as the carbon atom bonded to each bromine atom and each bromine atom is defined as the
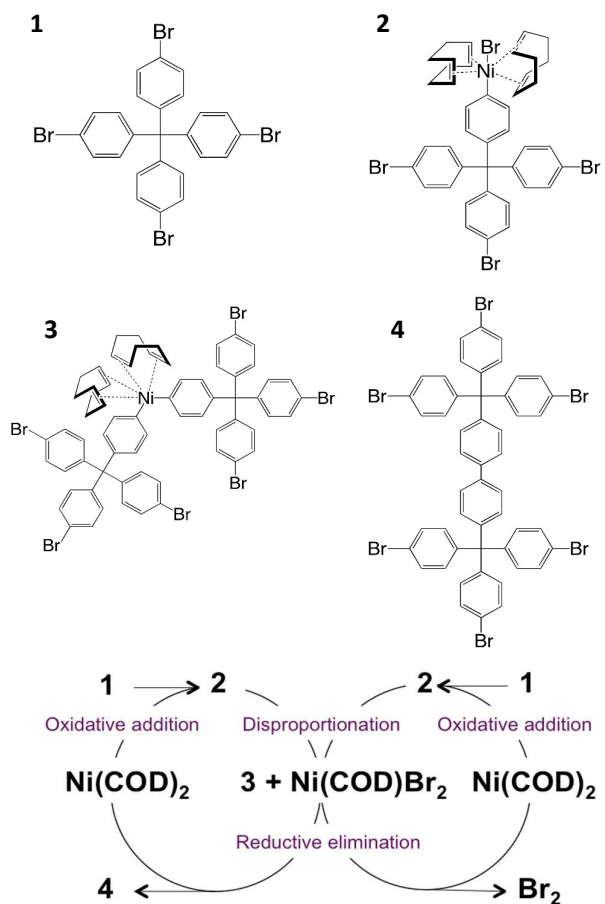

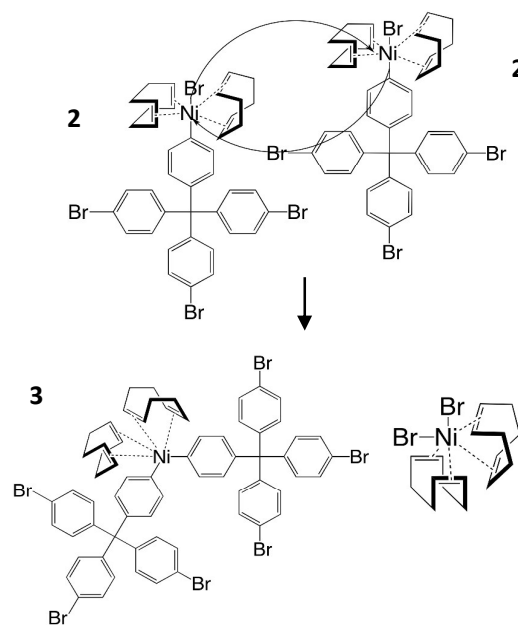Fig 1. The catalytic mechanism of the PAF framework formation.

Fig 2. The disproportionation of **2** to give **3** and Ni(COD)$_2$Br$_2$

leaving group. The AMBUILD code seeds an initial simulation cell with PAF building blocks and DMF solvent molecules in randomly assigned positions. A molecular dynamics (MD) simulation is then undertaken with regular structural sampling for bond formation. Bond formation is generated through a *Zip* test. The HOOMD-blue GPU-based code[36-38] is used as the MD engine, enabling long simulation times and easy integration with the Python code. Consecutive PAF building units are seeded into the system interspersed with MD simulations. At each step *Zip* testing is undertaken. Any end group atom pair that is within a set distance criteria is tested to ensure that their bond vectors are within a set angle criteria. Fig. S1 shows the bonding criteria diagrammatically. If a potential bond is found that fits the bonding criteria then a bond is formed and the geometry of the bond is optimized before the structure is subjected to additional MD simulation loops. Optimisation of the structure geometry uses the Fast Inertial Relaxation Engine (FIRE) rigid-body minimiser within HOOMD-blue.[38] The bromine leaving groups are removed from the simulation cell. A full description of the automated generation process can be found in the supporting information. This mimics network formation mechanism (2).

In this study, we use the AMBUILD code to further assess the framework generation process by probing the influence of the bonding criteria and the simulation process. The aspects of the framework generation process to be assessed are: (i) Molecular dynamic (MD) steps after each seed; (ii) solvent templating; (iii) the end group distance; (iv) the angle between end groups; and (v) cluster formation. Full computational details of each part can be found in supporting information. In parts (i), (ii), (iii) and (iv) we model network formation mechanism (2) and (4). Therefore we start with a simulation cell filled with solvent and no PAF building units. We gradually *Seed* the PAF build units and hence gradually increase the concentration of the PAF build units as the simulation proceeds.

(i) MD: The amount of MD after each seed step can influence the structure generation mechanism if significant re-arrangement of the PAF build units is required, for example for solvent templating. The MD allows the system to sample configurational space to find lower energy configurations. We start with a simulation cell of 50 x 50 x 50 Å that is filled with DMF molecules. Consecutive PAF building units are seeded into the system interspersed with MD simulations. At each step a bonding test is undertaken. If a bond is formed then the structure is optimised. Three different MD schemes are used with 1, 10, or 50 MD loops undertaken at each cycle. Each MD loop is an NVT MD simulation consisting of 100000 steps with a timestep of 0.5 fs.

(ii) Solvent Templating: Solvent templating is believed to aid in the generation of an open framework by blocking void space between framework strands and hence preventing network interpenetration. Here we test this effect by assessing the influence of two solvents: DCM and DMF. We start with a simulation cell of 50 x 50 x 50 Å that is filled with either DMF or DCM molecules. 10 MD loops are undertaken at each

AMBUILD cycle. Each MD loop is an NVT MD simulation consisting of 100000 steps with a timestep of 0.5 fs.

(iii) End-group distance: Large distances between end-groups enable the code to generate the framework more efficiently but can result in structurally impossible configurations. The distance between end-groups should reflect the catalytic mechanism. The minimal distance in the disproportionation mechanism will be determined by the width of the COD ligands. Assessment of the optimised $Ni(COD)_2BrR$ structure reveals that the radius of the Ni-COD ligands within the complex is between 3 and 5 Å. We have therefore investigated end-group distances between 3 and 15 Å to reflect the closest possible distance and the likely distance. We start with a simulation cell of 50 x 50 x 50 Å that is filled with DMF molecules. Consecutive PAF building units are seeded into the system interspersed with MD simulations. At each step bonding test is undertaken. If a bond is formed then the structure is optimised. 10 MD loops are undertaken at each AMBUILD cycle. Each MD loop is an NVT MD simulation consisting of 100000 steps with a timestep of 0.5 fs.

(iv) End group angle: The optimal angle at which the Br groups are relative to each other is dictated by the (i) the catalyst and (ii) the resulting structure of the node-to-node fragment. The optimal structure for the catalyst is with the vector of the catalyst-Br end groups at 0°, i.e. directly parallel. However, the resulting Ph-Ph groups are fixed into position by the framework and so the resulting fragment will not be structurally possible. Here we have taken angles between 10 and 100°. We start with a simulation cell of 50 x 50 x 50 Å that is filled with DMF molecules. Consecutive PAF building units are seeded into the system interspersed with MD simulations. At each step bonding test is undertaken. If a bond is formed then the structure is optimised. 10 MD loops are undertaken at each AMBUILD cycle. Each MD loop is an NVT MD simulation consisting of 100000 steps with a timestep of 0.5 fs.

(v) Cluster formation: Here, we model network formation mechanism (3), a step-by-step cluster formation mechanism. This mechanism may occur due to low concentrations of building block and high solubility of the resulting cluster meaning that the cluster is able to grow to larger sizes before precipitation occurs. To assess larger cluster sizes, we use a simulation cell of 300 x 300 x 300 Å with no solvent molecules included. Simulations of this size including solvent were not possible so we also use smaller simulation cells of 50 x 50 x 50 Å with and without DMF solvent molecules included. This means that potential templating effects of solvent on cluster growth can be investigated. Although this also means that only smaller cluster sizes or clusters that are able to bond across the periodic boundary are investigated. The generation of each of these smaller systems is repeated three times. Consecutive PAF building units are grown into the system interspersed with MD simulations. At each step bonding test is undertaken. If a bond is formed then the structure is optimised. 10 MD loops are undertaken at each AMBUILD cycle. Each MD loop is an NVT MD simulation consisting of 100000 steps with a timestep of 0.5 fs. Here we chose a number of different structural

parameters and we allow the simulation to run for a longer time period.

Results and Discussion

For amorphous materials, an exact structural model is not possible and hence we seek representative structures rather than a definitive model. There is little experimental data to which we can compare the generated models and therefore a holistic approach is taken whereby the models are compared to a number of different chemical and structural features. Experimentally, a weight percentage of Br atoms of less than 1% is observed. Here we observe the weight percentage of the system of Br (excluding solvent) as the framework is generated as a mechanism by which we can follow the progress and efficiency of the framework construction process. At each step of the generation process, additional building blocks are added to the simulation cell and so the weight percentage of bromine of the total cell can go up as well as down depending upon the amount *Seeded* and the number of successful *Zip* steps.

(i) MD: Fig. 3a. Shows the weight percentage of Br atoms within the simulation cell as a function of generation process step for a model with 1 MD step (Model-1), 10 MD steps (Model-2), and 50 MD steps (Model-3). We can see that there is little difference between the three models. We can therefore conclude that the amount of MD makes little difference on the resulting structure of the PAF framework. We therefore choose to use 10 MD steps for future framework generation processes.

(ii) Solvent Templating: Fig. 3b. Shows the weight percentage of Br atoms within the simulation cell as a function of generation process step for a model with DMF solvent (Model-4) and a model with DCM solvent (Model-5). We can see that initially the systems follow the same path but diverge after 10 steps with Model-4 having a lower weight percentage of Br. The biggest difference between the two models is at step 21 where Model-4 has 45.7 wt% Br and Model-5 has 17.8 wt% Br. Towards the end of the simulation run at steps 80-90, the two models have a similar weight percentage of Br. Assessing the structure of the two models at step 20, we find examples of solvent templating for Model 4 and for Model-5. For Model-4, a DCM molecule occupies the space between three PAF units that surround the centrally located DCM molecule in a triangular orientation. Similarly to previous work, we find that 4-6 DMF molecules occupy regions between four or six PAF build units respectively keeping the PAF build units separated. An example of the solvent templating observed for Model-4 and Model-5 is shown in Fig. 4.

The radial distribution function (RDF) for the central tetrahedral carbon atom of the PAF build unit was calculated at a number of stages during the framework growth for Model-4 and Model-5 and are shown in Fig SI4. For open framework structures, we would expect that the distance between tetrahedral carbons will be large with minimal distance being that of the distance between tetrahedral carbon atoms that are directly connected through the biphenyl linker. For networks that have a high degree of network
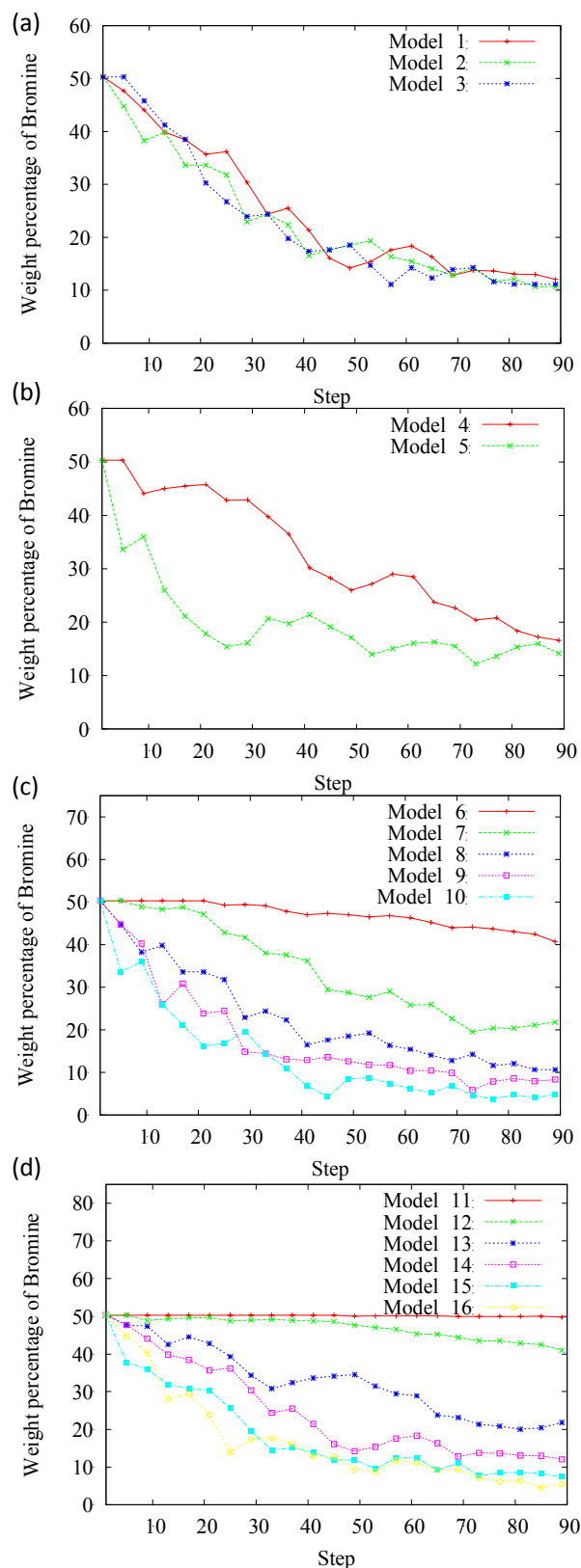

Fig 3. The weight % of Br of the PAF network as a function of build step for changing parameters:(a) amount of MD; (b) solvent; (c) end group distance; and (d) end group angle.

interpenetration, we expect to see a range of distances between tetrahedral carbon atoms with distances smaller than those defined by the directly connected tetrahedral carbon atoms. At the start of the structure generation process for Model-4 (DMF) there is a broad distribution of the PAF build units throughout the simulation cell at distances from 10 Å through to 24 Å. Whereas for Model-5 (DCM), there is a sharp peak centred at 10 Å and a set of peaks centred around 16 Å. As the structure generation process proceeds, the peaks become broader with smaller distances arising. For Model-4, the PAF build units come closer together, and hence react initially more quickly. However, a denser structure is formed with network interpenetration evident. For Model-5, the PAF build units are spaced out more within the simulation cell, this may slow down the reaction rate of network formation but allows the PAF build units to generate a more open framework structure.

(iii) End-group distance: Assessment of the Ni(COD)$_2$BrR complex, **2** showed that the COD ligand is large and bulky and extends out around the Ni metal atom to a distance of approximately 5 Å. This means that the closest distance that two complexes of **2** are able to get to other is ~ 10 Å. We can envisage that this distance of 10 Å will also take into account the disproportionation complex intermediates.

Fig. 3c. Shows the weight percentage of Br atoms within the simulation cell as a function of generation process step for Model-6 (end group distance of 3 Å), Model-7 (end group distance of 6.5 Å), Model-8 (end group distance of 10 Å), Model-9 (end group distance of 12 Å), and Model-10 (end group distance of 15 Å). For Model-6, the weight percentage of Br never goes lower than 40.7 wt%. This is because the PAF build molecules do not get close enough for bonds to be found during the zip test and therefore a network is unable to form. A similar plot is observed for Model-7, although the weight percentage of Br does reduce towards the end of the simulation. This is because the framework is able to become large enough within the simulation cell constraints that bonds are more likely to form. For Model-8, -9 and -10, a similar plot is observed for each with the weight percentage of Br being lower than 10.7 wt%. This demonstrates that above 10 Å end group distance the bonds are more likely to form.

Fig. S3 shows the weight percentage of bromine at the end of the network generation process as a function of the bonding distance zip criteria between end groups. The weight percentage of bromine at the end of the network generation process quickly drops as the bonding criteria distance is increased from 3 Å to 9 Å. Above 9 Å, the weight percentage of bromine does not drop as quickly.

(iv) End Group Angle: Fig. 3d Shows the weight percentage of Br atoms within the simulation cell as a function of generation process step for Model-11 (10°), Model-12 (30°), Model-13
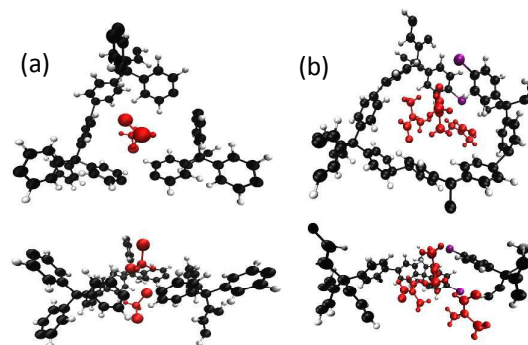

Fig 4. Examples of solvent templating during the network generation process (a) DCM (b) DMF.

(50°), Model-14 (70°), Model-15 (90°), and Model-16 (100°). Model-11 shows no reduction in Br weight percentage showing that no bonds were formed during the simulation. Model-12 shows a similar profile but with a small drop in the weight percentage at the end of the simulation showing that a small number of bonds were able to form. Model-13 shows a steady decrease but flattens out at the end of the simulation as more PAF build units are seeded into the simulation but no bonds are formed. Model-14 shows a steady decrease that continues to the end of the simulation. Model-15 and Model-16 both show an initial steep drop in the weight percentage of Br. The weight percentage continues to drop steadily towards the end of the simulation.

Fig. S4 shows the weight percentage of bromine at the end of the network generation process as a function of the angle zip criteria between end groups. The weight percentage of bromine at the end of the network generation process drops as the bonding criteria angle is increased from 10° to 30°. Above 30°, the weight percentage of bromine drops quickly before tailing off and dropping steadily from 70° to 100°.

The wider end-group angles means that a larger number of end groups can be found and allow more bonds to form. It should be noted that the wider angles allow end groups to form bonds at a wider range of angles and does not limit the lower angle possibilities.

(v) Cluster formation: Fig. S5. Shows the weight percentage of Br atoms within the simulation cell as a function of generation process step for Model-17 (end group distance = 8 Å and end group angle = 70°), Model-18 (end group distance = 8 Å and end group angle = 90°), Model-19 (end group distance = 8 Å and end group angle = 100°), Model-20 (end group distance = 12 Å and end group angle = 70°), Model-21 (end group distance = 12 Å and end group angle = 90°), and Model-22 (end group distance = 12 Å and end group angle = 100°). All models show a steep initial drop in the weight percentage of Br followed by a steady decrease. Model-18, -19, -21 and -22 were allowed to continue, with the weight percentage of Br steadily dropping to between 10 wt% and 15 wt%.
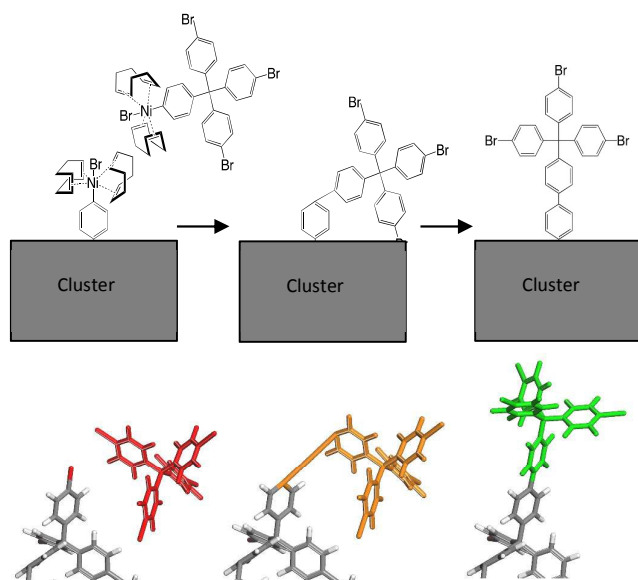
Fig 5. The 'snap-out' mechanism by which it is proposed that the relatively rigid PAF build units optimise their linker structure to adopt a structure close to its thermodynamic minima. Top-schematic of the snap-out mechanism. Bottom- snap shots from a *Zip* step. The initial starting position of the building block is shown in red, a bond is formed between the cluster and the building block, shown in orange. After optimisation, the building block has re-orientated due to the rigidity of the C(Ph)-C(Ph) bond resulting in the building block snapping out away from the cluster.

Model-22 had the lowest weight percentage of Br at 10 wt% and was allowed to continue to 15,000 steps where a weight percentage of Br of ~6 wt% was found. Fig S6a shows the full cluster growth for Model-22. The cluster grew to fill the 300x300x300 Å simulation cell. Fig S6b shows the weight percentage of Br atoms within the simulation cell as a function of generation process step for Model-22. Fig S6b shows the weight percentage of Br atoms within the simulation cell as a function of generation process step for the cluster growth from the point at which the cluster fills the simulation cells and is able to bond with its cluster image. Fig. S7 shows the cluster structure as the network is growing. The cluster grows outwards in a roughly spherical shape. At several points during the growth, a more linear strand of the PAF polymer extends outwards. This increases the total weight % of bromine, as the end groups of the strand are not able to bond due to there being no neighbouring end groups within the AMBUILD distance criteria. At some point the strand is able to bond back towards the bulk of the cluster by becoming sufficiently long and flexible or that PAF build units are grown to end groups within the strand that are then able to bond to the bulk of the cluster.

It is noted that after the grow step and subsequent optimisation, the PAF build units are all well optimised to positions close to the C(Ph)-C(Ph) bond orientation minima with little bending of the PAF build unit relative to the bulk of
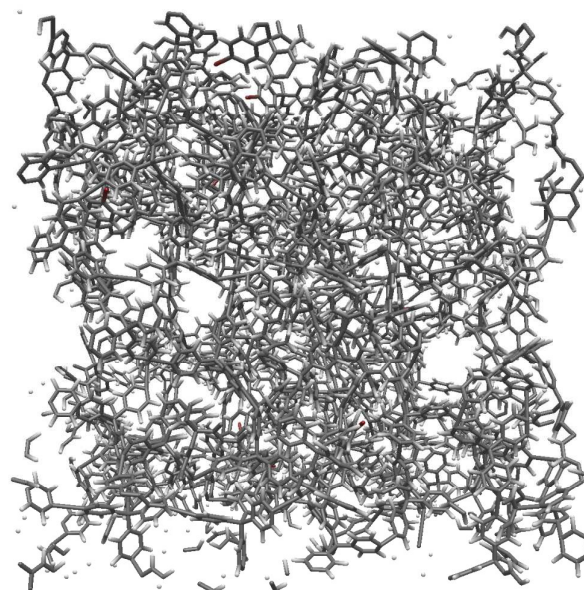

Fig 6. Model-25-2. Model constructed via a step-by-step mechanism in a unit cell of 50 Å x 50 Å x 50 Å. A final weight percentage of Br of 1.68 wt% is obtained.

the cluster. This due to the relative rigidity of the C(Ph)-C(Ph) bond meaning that any PAF build units that are grown on to the cluster will 'snap-out' away from the cluster regardless of what orientation they are initially grown in, Fig. 5. This importantly reduces the degree of network interpenetration within the cluster as it means that all new end groups are pointing out and away from the bulk of the cluster. This 'snap-out' mechanism may not occur for other more flexible linking groups, including, for example, PAF-11.[39]

Depending upon the dispersion of the catalyst within the system, the clusters may grow to a range of different sizes before being able to react and bond to each other. This is replicated in our models by changing the size of the simulation cell and the number of PAF build units that are initially seeded. We change the simulation cell size from 50 x 50 x 50 Å (Model-26), to 75 x 75 x 75 Å (Model-27), to 100 x 100 x 100 Å (Model-28) each with one PAF build unit seeded. AS the size of the cluster is increased, the weight percentage of Br increases from 2.73 wt%, to 4.56 wt%, to 5.47 wt% respectively. Smaller unit cells result in cluster growth quickly crossing the periodic boundary of the cell and bonding to its image. This results in a highly condensed network but with a higher density. Due to the large number of image-image bonding, some of the bonds between the PAF build units are stretched, as they cannot be reduced due to the cell constraints.

The number of seeded PAF build units was increased from 10 (Model-29), 25 (Model-30), 50 (Model-31), 75 (Model-32), to 100 (Model-33). The final weight percentage of Br is similar between all models at 1.93 – 2.75 wt%.

Polymer Formation Mechanism

The resultant polymer structures will now be assessed with respect to the polymer formation mechanisms discussed earlier.

Mechanisms (1) Instantaneous network formation, (2) Condensed step-by-step, and (4) Templating, are simulated by the generation of models-1 to -16. During the generation of these models we see no instantaneous networks forming despite the ability to do so. The networks grow in a step-by-step manner, small oligomers are formed during the early stages of the network growth with these bonding to form larger fragments and then ultimately the polymer network. No network interpenetration is observed. Solvent templating appears to have some influence on the mechanism of the network formation in holding the building blocks further apart during the generation process. Although the final resultant weight percentage of Br does not differ, this effect may be significant in the real system, where subtle effects can have large influence.

In general, the weight percentage of Br is high with most values between 4.8 and 20 wt%, significantly higher than the observed experimental value of less than 1 wt%. Overall, the density of the models is consistent with models identified in earlier studies [21] with ranges between 0.36 and 0.48 g cm^3.

Models-16 to -33 simulates the polymer generation mechanism (3) Cluster step-by-step. For large isolated clusters with no cluster-cluster bonding, models-17 to -22, the overall weight percentage of Br is high at between 5.6 and 13.8 wt%. It is conceivable that the clusters continue to grow to the μm scale and that the internal weight percentage of the Br is much reduced compared to that at the edges of the cluster. To test this, an internal section of the cluster formed in Model-22 was selected at random and the respective weight percentage of Br was calculated to be 2.77 wt%, lower than the overall density of 5.96 wt%. Where clusters are able to bond together either across the periodic boundaries or where multiple clusters are generated within a single cell, models-23 to 33, the weight percentage of Br is low with the lowest value achieved of 1.68 wt% (Model-25, shown in Fig. 6) close to the experimental value of less than 1 wt%. However, it is noted that the density is higher (Model-25 has a density of 0.76 g cm^{-3}) than the density of other models generated in previous studies that replicate the experimental porous properties (amorphous model density of 0.37 g cm^{-3}).[21]

Conclusions

The step-by-step cluster mechanism modelled here closely replicates the experimental weight percentage of Br and the non-interpenetrated network structure. However, it does not replicate the extremely low densities that are observed experimentally. Solvent interactions also influence the mechanism of the network formation. We believe that a combination of solvent templating and step-by-step cluster formation that was not possible to model here for larger scale systems, may take us a step closer to being able to rationalise the formation mechanism of ultra porous PAF materials. This

may help to design targeted future systems for high surface area materials.

Importantly, we have identified a rationalisation for the lack of network interpenetration observed in the PAF material involving a 'snap-out' mechanism by which the relatively rigid PAF linker enforces the PAF build units to adopt their structures close to their thermodynamic minima structures. This also rationalises why materials with more flexible linkers, for example CMP materials, form more dense, highly interpenetrated networks.

Acknowledgements

Notes and references

1. M. Eddaoudi, D. B. Moler, H. Li, B. Chen, T. M. Reineke, M. O'Keefe and O. M. Yaghi, *Acc. Chem. Res.*, 2001, **34**, 319-330.

2. S. Kitigawa, R. Kitaura and S. Noro, *Angew. Chem., Int. Ed.*, 2004, **43**, 2334-2375.

3. S. S. Han and W. A. Goddard, *Journal of the American Chemical Society*, 2007, **129**, 8422-8423.

4. A. P. Côté, A. I. Benin, N. W. Ockwig, M. O'Keeffe, A. J. Matzger and O. M. Yaghi, *Science*, 2005, **310**, 1166-1170.

5. J. R. Hunt, C. J. Doonan, J. D. LeVangie, A. P. Cote and O. M. Yaghi, *J. Am. Chem. Soc.*, 2008, 11872-11873.

6. A. P. Cote, H. M. El-Kaderi, H. Furukawa, J. R. Hunt and O. M. Yaghi, *J. Am. Chem. Soc.*, 2007, **129**, 12914 - 12915.

7. H. M. El-Kaderi, J. R. Hunt, J. L. Mendoza-Cortes, A. P. Cote, R. E. Taylor, M. O'Keefe and O. M. Yaghi, *Science*, 2007, **316**, 268-272.

8. S. Wan, J. Guo, J. Kim, H. Ihee and D. Jiang, *Angew. Chem. Int. Ed.*, 2008, **47**, 1-5.

9. J. Germain, J. M. J. Fréchet and F. Svec, *Small*, 2009, **5**, 1098-1111.

10. R. Dawson, A. I. Cooper and D. J. Adams, *Progress in Polymer Science*, 2012, **37**, 530-563.

11. L. J. Barbour, *Chemical Communications*, 2006, 1163-1168.

12. A. K. Cheetham, G. Ferey and T. Loiseau, *Angew. Chem. Int. Ed.*, 1999, 3268 - 3292.

13. J. T. A. Jones, T. Hasell, X. Wu, J. Bacsa, K. E. Jelfs, M. Schmidtmann, S. Y. Chong, D. J. Adams, A. Trewin, F. Schiffman, F. Cora, B. Slater, A. Steiner, G. M. Day and A. I. Cooper, *Nature*, 2011, **474**, 367-371.

14. H. Furukawa, N. Ko, Y. B. Go, N. Aratani, S. B. Choi, E. Choi, A. O. Yazaydin, R. Q. Snurr, M. O'Keeffe, J. Kim and O. M. Yaghi, *Science*, 2010, **329**, 424-428.

15. C. D. Wood, B. Tan, A. Trewin, H. Niu, D. Bradshaw, M. J. Rosseinsky, Y. Z. Khimyak, N. L. Campbell, R. Kirk, E. Stoeckel and A. I. Cooper, *Chem. Mat.*, 2007, **19**, 2034-2048.

16. T. Ben, H. Ren, S. Ma, D. Cao, J. Lan, X. Jing, W. Wang, J. Xu, F. Deng, J. Simmons, S. Qiu and G. Zhu, *Angewandte Chemie International Edition*, 2009, **48**, 9457-9460.

17. A. Trewin and A. I. Cooper, *Angewandte Chemie International Edition*, 2010, **49**, 1533-1535.

ARTICLE

Journal Name

18. J. Jiang, F. Su, A. Trewin, C. D. Wood, N. L. Campbell, H. Niu, C. Dickinson, A. Y. Ganin, M. J. Rosseinsky, Y. Z. Khimyak and A. I. Cooper, *Angew. Chem. Int. Ed.*, 2007, **46**, 1 - 5.

19. J. Weber and A. Thomas, *Journal of the American Chemical Society*, 2008, **130**, 6334-6335.

20. N. B. McKeown and P. M. Budd, *Chem. Soc. Rev.*, 2006, **35**, 675-683.

21. J. M. H. Thomas and A. Trewin, *The Journal of Physical Chemistry C*, 2014, **118**, 19712-19722.

22. J.-X. Jiang, F. Su, A. Trewin, C. D. Wood, H. Niu, J. T. A. Jones, Y. Z. Khimyak and A. I. Cooper, *J Am Chem Soc*, 2008, doi: ja-2008-010176.R010171; in press.

23. A. Trewin, D. J. Willock and A. I. Cooper, *The Journal of Physical Chemistry C*, 2008, **112**, 20549-20559.

24. H. Tobita and A. E. Hamielec, *Macromolecules*, 1989, **22**, 3098-3105.

25. H. Tobita, *Macromolecules*, 1993, **26**, 5427-5435.

26. B. D. Fairbanks, T. F. Scott, C. J. Kloxin, K. S. Anseth and C. N. Bowman, *Macromolecules*, 2009, **42**, 211-217.

27. C. Decker, *Polymer International*, 2002, **51**, 1141-1150.

28. A. Trewin, D. J. Willock and A. I. Cooper, *J. Phys. Chem. C.*, 2008, 20549-20559.

29. S. H. Garofalini and G. Martin, *The Journal of Physical Chemistry*, 1994, **98**, 1311-1316.

30. A. Laybourn, R. Dawson, R. Clowes, T. Hasell, A. I. Cooper, Y. Z. Khimyak and D. J. Adams, *Polymer Chemistry*, 2014, **5**, 6325-6333.

31. T. Yamamoto and T.-a. Koizumi, *Polymer*, 2007, **48**, 5449-5472.

32. T. Ben and S. Qiu, *CrystEngComm*, 2013, **15**, 17-26.

33. YAMAMOTO, T., WAKABAYASHI, S., OSAKADA and K., *Mechanism of C-C coupling reactions of aromatic halides, promoted by Ni(COD)[2] in the presence of 2,2'-bipyridine and PPh[3], to give biaryls*, Elsevier, Lausanne, SUISSE, 1992.

34. M. Valiev, E. J. Bylaska, N. Govind, K. Kowalski, T. P. Straatsma, H. J. J. Van Dam, D. Wang, J. Nieplocha, E. Apra, T. L. Windus and W. A. de Jong, *Computer Physics Communications*, 2010, **181**, 1477-1489.

35. S. Grimme, J. Antony, S. Ehrlich and H. Krieg, *The Journal of Chemical Physics*, 2010, **132**, 154104-154119.

36. http://codeblue.umich.edu/hoomd-blue.

37. J. A. Anderson, C. D. Lorenz and A. Travesset, *Journal of Computational Physics*, 2008, **227**, 5342-5359.

38. T. D. Nguyen, C. L. Phillips, J. A. Anderson and S. C. Glotzer, *Computer Physics Communications*, 2011, **182**, 2307-2313.

39. Y. Yuan, F. Sun, H. Ren, X. Jing, W. Wang, H. Ma, H. Zhao and G. Zhu, *Journal of Materials Chemistry*, 2011, **21**, 13498-13502.